UC Irvine
UC Irvine Previously Published Works

Title

A Computational Study of a Data Assimilation Algorithm for the Two-dimensional Navier-Stokes Equations

Permalink

Journal

ISSN

Authors

Gesho, Masakazu
Olson, Eric
Titi, Edriss S

Publication Date

DOI

Peer reviewed

A Computational Study of a Data Assimilation Algorithm for the Two-dimensional Navier–Stokes Equations

Masakazu Gesho[*]   Eric Olson[†]   Edriss S. Titi[‡§]

May 3, 2015

Abstract

We study the numerical performance of a continuous data assimilation (downscaling) algorithm, based on ideas from feedback control theory, in the context of the two-dimensional incompressible Navier–Stokes equations. Our model problem is to recover an unknown reference solution, asymptotically in time, by using continuous-in-time coarse-mesh nodal-point observational measurements of the velocity field of this reference solution (subsampling), as might be measured by an array of weather vane anemometers. Our calculations show that the required nodal observation density is remarkably less that what is suggested by the analytical study; and is in fact comparable to the *number of numerically determining Fourier modes*, which was reported in an earlier computational study by the authors. Thus, this method is computationally efficient and performs far better than the analytical estimates suggest.

Keywords: Continuous data assimilation; determining nodes; signal synchronization; two-dimensional Navier–Stokes equations; downscaling.

AMS Classification: 35Q30; 93C20; 37C50; 76B75; 34D06.

[*]Department of Mathematics, University of Wyoming, 1000 E. University Ave, Dept. 3036, Laramie, WY 82071, USA. *email:* mgesho@uwyo.edu

[†]Department of Mathematics and Statistics, University of Nevada, Reno, NV 89557, USA. *email:* ejolson@unr.edu

[‡]Department of Mathematics, Texas A&M University, 3368–TAMU, College Station, TX 77843, USA. *email:* etiti@math.tamu.edu

[§]The Department of Computer Science and Applied Mathematics, Weizmann Institute of Science, Rehovot 76100, Israel. *email:* edriss.titi@weizmann.ac.il

1 Introduction

The goal of data assimilation is to provide a more accurate representation of the current state of a dynamical system by combining observational data with model dynamics. This allows the influences of new data to be incorporated into a numeric computation over time. Data assimilation is widely used in the climate sciences, including weather forecasting, environmental forecasting and hydrological forecasting. Additional information and historical background may be found in Kalnay [13] and references therein.

In 1969 Charney, Halem and Jastrow [5] proposed a method of continuous data assimilation in which observational measurements are directly inserted into the mathematical model as it is being integrated in time. To fix ideas, let us suppose that the evolution of u is governed by the dynamical system

$$\frac{du}{dt} = \mathcal{F}(u), \qquad u(t_0) = u_0 \tag{1}$$

and the observations of u are given by the time series $p(t) = Pu(t)$ for $t \in [t_0, t_*]$, where P is an orthogonal projection onto the low modes. In this context, the method proposed in [5] for approximating u from the observational data is to solve for the high modes

$$\frac{dq}{dt} = (I - P)\mathcal{F}(q + p), \qquad q(t_0) = q_0 \tag{2}$$

where q_0 is an arbitrarily chosen initial condition and $q + p$ represents the resulting approximation of u. Note that if $q_0 = (I - P)u_0$ then $p + q = u$ for all time; however, data assimilation is applied when u_0 is not known.

Algorithm (2) was studied by Olson and Titi in [17] and [18] for the two-dimensional incompressible Navier–Stokes equations

$$\begin{cases} \dfrac{\partial u}{\partial t} - \nu\Delta u + (u \cdot \nabla)u + \nabla p = f \\ \qquad\qquad\qquad \nabla \cdot u = 0 \end{cases} \tag{3}$$

on the domain $\Omega = [0, L]^2$, equipped with periodic boundary conditions and zero spatial average with initial condition $u(x, t_0) = u_0(x)$ for $x \in [0, L]^2$. Observational measurements were represented by $P = P_h$, where P_h is the orthogonal projection onto the Fourier modes $\exp(2\pi i k \cdot x/L)$ with wave numbers $k \in \mathbf{Z}^2 \setminus \{0\}$ such that $0 < |k| \le L/h$. Here $\nu > 0$ is the kinematic viscosity, $p(x, t)$ is the pressure and $f(x)$ is a time-independent body force with zero spatial average acting on the fluid. For simplicity, it was assumed, as we shall here, that $\nabla \cdot f = 0$.

The two-dimensional incompressible Navier–Stokes equations are amenable to mathematical analysis while at the same time they posses non-linear dynamics similar to the partial differential equations that govern realistic physical phenomenon. Using the functional notation of Constantin and Foias [6], see also Temam [20] or Robinson [19], write (3) in the form (1) by setting

$$\mathcal{F}(u) = -\nu A u - B(u, u) + f \qquad (4)$$

where A and B are the continuous extensions of the operators given by

$$A = -P_\sigma \Delta u \qquad \text{and} \qquad B(u, v) = P_\sigma(u \cdot \nabla v)$$

when u, v are smooth divergence-free L-periodic functions, and P_σ is the Leray–Helmholtz projector. We recall that

$$P_\sigma(u) = \sum_{k \in \mathbf{Z}^2 \setminus \{0\}} \left\{ u_k - \frac{k \cdot u_k}{|k|^2} k \right\} \exp(2\pi i k \cdot x / L)$$

and also that $A: V^1 \to V^{-1}$ and $B: V^1 \times V^1 \to V^{-1}$ where V^α is the closure of $\mathcal{V}$, the space of zero-average $\mathbf{R}^2$-valued divergence-free L-periodic trigonometric polynomials, with respect to the norm

$$\|u\|_{V^\alpha} = L^2 \sum_{k \in \mathbf{Z}^2 \setminus \{0\}} |k|^{2\alpha} |\hat{u}_k|^2.$$

For notational convenience we shall write $V = V^1$ throughout the remainder of this paper.

Consider the data assimilation method given by (2). Using the theory of determining modes it was shown as Theorem 1.5 in [17] that if h satisfies

$$\frac{L^2}{h^2} \geq c_1 G \qquad (5)$$

then $\|u(t) - p(t) - q(t)\|_V \to 0$, exponentially fast as $t \to \infty$. Here c_1 is a universal constant and $G = (L/2\pi\nu)^2 \|f\|_{L^2}$ is the Grashof number. Computations in [18] considered a fixed forcing function $f = f_{121}$ scaled to obtain different values for G. In that work the subscript 121 was used to indicate that the force was supported on an annulus around $k^2 = 121$ in Fourier space. More details on f are provided by equation (14) and Figure 1 below. For Grashof numbers between $500\,000$ and $60\,000\,000$ it was shown that the projection P_h onto the lowest 80 Fourier modes was necessary and sufficient to ensure numerically that $\|u(t) - p(t) - q(t)\|_V \to 0$, as $t \to \infty$. Since the rank of P_h scales as L^2/h^2, this is significantly less than the millions

3

suggested by the analytical bound (5). Thus, the data assimilation algorithm given by (2) performs far better than the analysis suggests. Note, however, that this algorithm is not suitable when the observations are given by nodal measurements of the velocity field.

An approach to data assimilation, for dynamics governed by equations (3) or equivalently (4), which is applicable to nodal observations, was introduced and analyzed by Azouani, Olson and Titi in [1]. Let I_h be a general interpolant observable satisfying the approximation identity inequality

$$\|u - I_h(u)\|_{L^2}^2 \leq \gamma_1 h^2 \|u\|_{H^1}^2 + \gamma_2 h^4 \|u\|_{H^2}^2. \tag{6}$$

Given $I_h(u(t))$ for $t \in [t_0, t_*]$, solve

$$\frac{dv}{dt} = \mathcal{F}(v) + \mu P_\sigma(I_h(u) - I_h(v)), \qquad v(t_0) = v_0, \tag{7}$$

where v_0 is an arbitrary initial condition. The constant μ is a relaxation (nudging) parameter which controls the strength of the feedback control (nudging term). In particular, the nudging term pushes the large spatial scales of the approximating solution v toward those of the reference solution u while the viscosity stabilizes and dissipates the fine spatial scales and any spillover into the fine scales caused by the nudging term. It follows from Theorem 2 equation (39) of [1] that if h and μ satisfy

$$\frac{L^2}{h^2} \geq \frac{c_0 L^2 \mu}{\nu} \geq c_2 G(1 + \log(1 + G)), \tag{8}$$

then $\|u(t) - v(t)\|_V \to 0$ as $t \to \infty$. Here c_2 is a universal constant and c_0 is a constant depending only on γ_1 and γ_2 of (6).

The number of nodal measurements needed to uniquely determine a solution to the two-dimensional Navier–Stokes equations, as $t \to \infty$, was found by Foias and Temam in [9] and further refined in Jones and Titi [12]. Up to a logarithmic correction, the analytic bounds given by (8) are the same as those given in [12]. In this paper we check the numerical performance of the data assimilation algorithm (7) using nodal measurements given by I_h for the same body forcing f considered in [18] scaled so that $G = 2\,500\,000$.

Let Q_i be disjoint squares that cover $[0, L]^2$ with centers x_i and sides of length $h = L/K$, where $K^2 = N$. An interpolant operator based on the nodal measurements $u(x_i, t)$, for $i = 1, 2, \ldots, N$, and $t \in [t_0, t_*]$, which satisfies (6) is

$$I_h(u)(x, t) = \mathcal{I}_h(u)(x, t) - \frac{1}{L^2} \int_{[0,L]^2} \mathcal{I}_h(u)(x, t) \, dx, \tag{9}$$

where

$$\mathcal{I}_h(u)(x, t) = \sum_{i=1}^{N} u(x_i, t) \chi_{Q_i}(x). \tag{10}$$

4

We also consider the smoothed interpolation

$$\tilde{I}_h(u)(x,t) = \widetilde{\mathcal{I}}_h(u)(x,t) - \frac{1}{L^2} \int_{[0,L]^2} \widetilde{\mathcal{I}}_h(u)(x,t)\,dx, \qquad (11)$$

where

$$\widetilde{\mathcal{I}}_h(u)(x,t) = \sum_{i=1}^{N} u(x_i,t)(\rho_\epsilon * \chi_{Q_i})(x), \qquad (12)$$

and $\rho_\epsilon(x) = \epsilon^{-2}\rho(x/\epsilon)$ with

$$\rho(\xi) = \begin{cases} K_0 \exp\left(\dfrac{1}{1-\xi_1^2} + \dfrac{1}{1-\xi_2^2}\right) & \text{for } |\xi_1|, |\xi_2| < 1 \\ 0 & \text{otherwise,} \end{cases} \qquad (13)$$

and

$$K_0^{-1} = \int_{-1}^{1}\int_{-1}^{1} \exp\left(\frac{1}{1-\xi_1^2} + \frac{1}{1-\xi_2^2}\right)d\xi_2\,d\xi_1.$$

To make the smoothing scale compatible with the resolution parameter we take $\epsilon = \eta h$ for some fixed $\eta > 0$. An analysis of a smoothed interpolant similar to $\tilde{I}_h$ appears in Appendix A of [1] for $\eta = 0.1$ and shows that $\tilde{I}_h$ satisfies (6). Note also that $\tilde{I}_h \to I_h$ as $\eta \to 0$. When η is between 0 and 1 the convolution reduces the high-frequencies that would otherwise be present in the Fourier series representation of the characteristic function χ_{Q_i}. Values of η greater than 1 blur nearby nodal measurements together. This further downscaling could be useful in the presence of noisy measurements, see for example [3]; however, the measurements studied here will be error free. In this work we vary η between 0.1 and 2.0 and find that $\eta = 0.7$ leads to near optimal performance for our data assimilation experiments.

In particular, our results show that $\|u(t) - v(t)\|_V \to 0$, as $t \to \infty$, when the resolution K of the observational measurements satisfies $K \geq 8$ and μ and η are appropriately chosen. Moreover, if $K \geq 9$ and $\eta = 0.7$, there is a wide range of values for μ such that the algorithm works well. Since 64 and 81 nodes are comparable in resolution to 80 Fourier modes, the numerical efficiency of algorithm (7), using nodal measurements, is comparable to algorithm (2) using Fourier modes [17, 18].

Rigorous mathematical analysis of the method of data assimilation studied computationally in this paper has recently been generalized to Bénard convection by Farhat, Jolly and Titi [7] where it was shown that only observational measurements of the velocity field is sufficient to recover the full reference solution, i.e., the velocity field and the temperature. Inspired by [7] Farhat, Lunasin and Titi [8] have recently improved the algorithm studied here, i.e. the one introduced in [1], by showing that it is sufficient to use

observational measurements of only one component of the velocity field to recover the full reference solution. Further implementation of this algorithm, for the subcritical surface quasi-geostrophic equation, has recently been established by Jolly, Martinez and Titi [11]. The algorithm studied here is also closely related the 3DVAR data assimilation method developed by Blömker, Law, Stuart and Zygalakis [4] for the Navier–Stokes equations and by Law, Shukla and Stuart [14] for Lorenz equations.

This paper is organized as follows. Section 2 describes the physical parameters, forcing and initial conditions used to generate the reference solution to the two-dimensional incompressible Navier–Stokes equations that we will be observing through nodal measurements of the velocity field. Section 3 reports our computational results, and section 4 gives details of our computational methods. The last section concludes that data assimilation of nodal measurements, by means of equation (7), as studied in this paper works computationally just as efficiently as equation (2) with Fourier modes.

2   The Reference Solution

To focus on how the smoothing and resolution of the observational measurements affect algorithm (7), as well as how to optimize the value of the relaxation (nudging) parameter μ, we fix the viscosity and the size of the periodic box so that

$$\nu = 0.0001 \qquad \text{and} \qquad L = 2\pi$$

for the remainder of this paper. We further perform all our simulations using the same reference solution $u(t)$ to the two-dimensional incompressible Navier–Stokes equations. As shown in [17] the spatial structure of the function f used to force the reference solution can have a significant effect on data assimilation. Therefore, to allow comparison with previous results, we use the exact same forcing function defined in [17], and further studied in [18], scaled such that $G = 2\,500\,000$ in our present computations.

This function f is supported on the annulus in Fourier space with wave numbers k such that $110 \leq k^2 \leq 132$. In particular,

$$f(x) = \sum_{110 \leq k^2 \leq 132} \hat{f}_k \exp(ik \cdot x) \tag{14}$$

with $\hat{f}_k = \overline{\hat{f}_{-k}}$ and $k \cdot \hat{f}_k = 0$, where the values of $\hat{f}_k$ are given by Table 1 in [18] scaled to obtain the desired Grashof number. Note that this forcing

is at length scales of about 1/11-th the size of the periodic box. This fact is further reflected in the level curves of

$$\operatorname{curl} f = \operatorname{curl}(f_1, f_2) = \frac{\partial f_2}{\partial x} - \frac{\partial f_1}{\partial y}$$

depicted in Figure 1 on the left.

Figure 1: Left are contours of $\operatorname{curl} f$; right are vorticity contours of u_0.
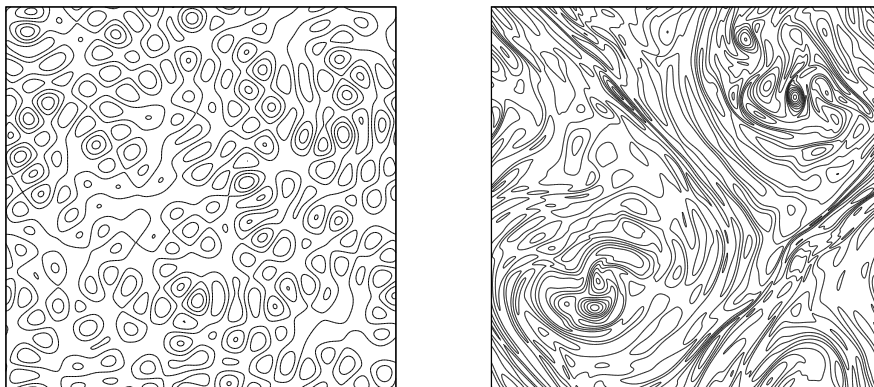
The initial condition u_0 used for our data assimilation experiments was obtained by solving (3) with zero initial condition at time $t = -25000$ until time $t = 0$. In terms of eddy turnover times, this ensures that more than 500 eddy turnovers have occurred before reaching $t = 0$. Integrating for this length of time ensures the initial condition u_0 lies close to the global attractor and therefore reflects the energetics of the forcing f. In particular, the way in which we initialized the solution at time $t = -25000$ is unimportant.

The vorticity contours $\omega_0 = \operatorname{curl} u_0$ of the initial condition u_0 are depicted in Figure 1 on the right. While the forcing f contains no Fourier modes with wave numbers k such that $|k| < 10$, the initial condition u_0 clearly possesses two large eddies the size of the box. These large box-filling eddies apparently result from the inverse cascade of energy in the two-dimensional Navier–Stokes equations. This can be seen more clearly by examining the energy spectrum of the reference solution.

Given a solution $u(t)$ to the two-dimensional Navier–Stokes equations for $t \in [0, T]$ where $T = 25\,000$ define the average energy spectrum as

$$E(r) = \frac{4\pi^2}{T} \int_0^T \sum_{k \in \mathcal{J}_r} |\hat{u}_k(t)|^2 dt \quad \text{where} \quad u(t) = \sum_{k \in \mathbf{Z}^2 \setminus \{0\}} \hat{u}_k(t) e^{ik \cdot x}$$

and $\mathcal{J}_r = \{\, k \in \mathbf{Z}^2 : r - 0.5 < |k| \le r + 0.5 \,\}$. For the reference solution described above with initial condition u_0 and time $t_0 = 0$, the average energy

7

spectrum appears in Figure 2. While we do not see the Kraichnan scaling of k^{-3} in the inertial range, we do see the Kolmogorov $k^{-5/3}$ scaling in the inverse cascade. Such spectra have been observed in other numerical experiments, see, for example, Xiao, Wan, Chen and Eyink [21]. In particular, the inverse cascade appears responsible for the box-filling eddies observed in the initial condition u_0 which persist for all times $t > 0$.

Figure 2: Time averaged energy spectrum of the reference solution.
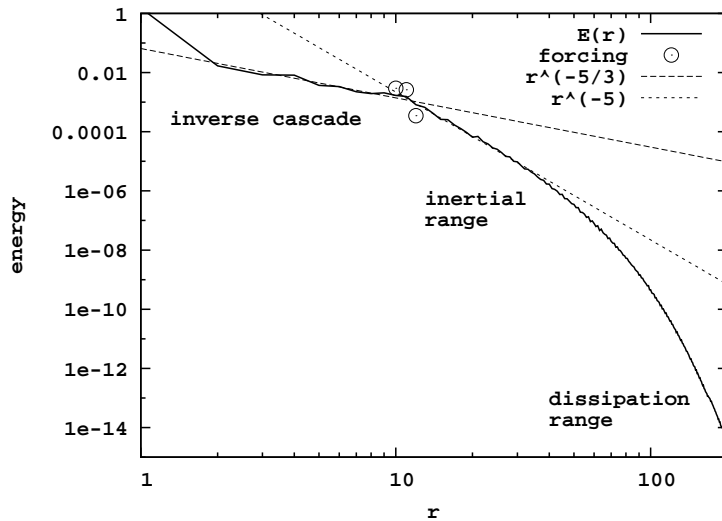
We compute the eddy turnover time for the reference solution as

$$\tau = 4\pi^2 \sum_{r=1}^{\infty} r^{-1} E(r) / \Big(\sum_{r=1}^{\infty} E(r) \Big)^{3/2} \approx 30.8$$

and conclude that our averages have been computed over $T/\tau \approx 812$ eddy turnovers. The spectrum of τf, which also has units of energy, has been plotted in Figure 2 as three circles to illustrate where the forcing lies in relation to the energy spectrum. Note that the forcing exactly divides the energy spectrum between the part which scales as $k^{-5/3}$ and the part which scales as k^{-5}.

Having, to some extent, described the reference solution that will be used in our numerical experiments, we now turn to our main point of study, the data assimilation of nodal measurements of the velocity field.

3 Nodal Observations of Velocity

We consider nodal observations $u(x_i, t)$, for $i = 1, \ldots, N$, of the reference solution u, that was computed according to the incompressible two-dimensional Navier–Stokes equations (3) and initialized with u_0 as described in Figure 1, and interpolate these measurements using the operator I_h defined by (9). The resulting equations for the approximating solution v may be written as

$$\frac{dv}{dt} + \nu Av + B(v, v) = f - \mu P_\sigma(I_h(u) - I_h(v)) \tag{15}$$

where v is initialized as $v_0 = 0$. Note that only the observations $I_h(u)$ of the reference solution u enter into the equations for computing for v. Also note that $\|u(0) - v(0)\|_V = \|u_0\|_V \approx 1.946$. Our goal now is to choose the resolution parameter h and the relaxation (nudging) parameter μ in such a way that $\|u(t) - v(t)\|_V \to 0$, numerically, as $t \to \infty$.

As discussed in [1], if μ is too small, the feedback control (nudging term) will be too weak to ensure the approximating solution converges to the reference solution. If μ is too large, then spill over into the fine scales becomes significant and again prevents recovery of the reference solution. Figure 3 illustrates each of these possibilities for $h = L/K$, where $K = 9$, using different values of μ.

Figure 3: The error $\|u(t) - v(t)\|_V$ versus t for $h = 0.6981$.
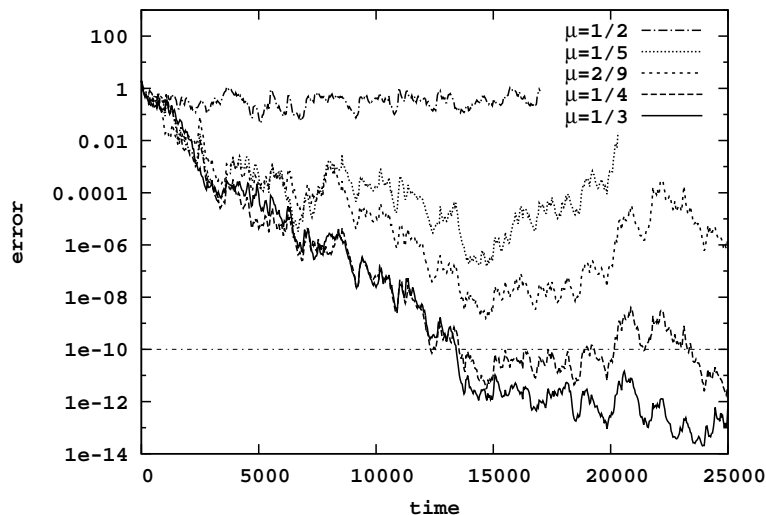
When $\mu = 1/2$ the relaxation (nudging) parameter is too large for the approximating solution to converge to the reference solution, and when $\mu =$

1/5 it is too small. However, the intermediate value $\mu = 1/3$ works with the error represented by $\|u(t) - v(t)\|_V$ falling below 10^{-10} by $t = 13\,417.8$. Note that, since the double-precision floating-point numbers used to represent the Fourier modes of u and v on the computer have only 15 digits of precision, we don't expect convergence of $\|u(t) - v(t)\|_V$ to exact zero over time.

For $\mu = 1/4$ the error falls below 10^{-10} at $T = 12\,327.1$, however, it rises again and it is not clear whether after $T = 23\,463.9$ the error finally stays below 10^{-10} or not. The value $\mu = 2/9$ shows an even more irregular pattern where $\|u(t) - v(t)\|_V$ exhibits a period of decay followed by a period of growth that covers six orders of magnitude. Fortunately, most of our parameter choices avoid these borderline cases and the corresponding error either converges towards zero and stays below 10^{-10} or shows few signs of converging and stays well above 10^{-10}.

To determine the values of h and μ for which it is possible to recover the reference solution to within numerical roundoff error we fix $\epsilon > 0$ and define

$$T_{\max} = \sup \left\{ t \in [0, T] : \|v(t) - u(t)\|_V \geq \epsilon \right\}$$

and

$$T_{\min} = \inf \left\{ t \in [0, T] : \|v(t) - u(t)\|_V \leq \epsilon \right\}$$

Let $T_{\max} = 0$, when the supremum is over the empty set, and $T_{\min} = \infty$ when the infimum is over the empty set. When $\|v(T) - u(T)\|_V \geq \epsilon$ further set $T_{\max} = \infty$ to ensure $T_{\max} \geq T_{\min}$. Inspired by Figure 3 we also define

$$\varepsilon_{\mathrm{avg}} = \frac{1}{T - T_0} \int_{T_0}^{T} \|v(t) - u(t)\|_V \, dt$$

and take $\epsilon = 10^{-10}$, $T = 25\,000$ and $T_0 = 2T/3$ for our numerics.

Table 1 shows the results of our computational experiments. Runs with $K = 8$ were also performed, however, no value of μ yielded a finite value for $T_{\max}$ or $T_{\min}$ or even an approximation for which the error $\|u(t) - v(t)\|_V$ fell below 10^{-2}. We conclude that $K = 9$ is the minimal resolution for which there exists a μ such that the error tends toward zero. At this minimal resolution only a narrow range of values for μ near $1/3$, result in an error which falls below 10^{-10}. When $K = 10$, there is a much greater range of corresponding values for μ that work well. In fact, when $K = 10$ all values of μ between $1/6$ and $1/2$ led to corresponding approximations $v(t)$ such that $\varepsilon_{\mathrm{avg}} \approx 3 \times 10^{-14}$. Since the double-precision floating-point numbers used to represent the Fourier modes of u and v on the computer have only 15 digits of precision, the fact that the error can approach 10^{-14} is remarkable. We again note, as is consistent with the analysis in [1], our numerical experiments do not recover the reference solution if μ is too small or too large.

10

Table 1: Data assimilation using I_h.

	$K = 9$			$K = 10$		
μ	$T_{\min}$	$T_{\max}$	$\varepsilon_{\mathrm{avg}}$	$T_{\min}$	$T_{\max}$	$\varepsilon_{\mathrm{avg}}$
0.0625	∞	∞	1.1	∞	∞	8.8×10^{-1}
0.125	∞	∞	3.9×10^{-1}	13754.5	17094.3	4.1×10^{-12}
0.154	∞	∞	2.4×10^{-1}	4331.1	4432.6	5.4×10^{-14}
0.167	∞	∞	2.4×10^{-1}	3965.0	4187.7	3.1×10^{-14}
0.182	∞	∞	1.5×10^{-1}	3320.1	3320.1	2.8×10^{-14}
0.2	∞	∞	3.5×10^{-2}	2825.2	2825.2	2.8×10^{-14}
0.222	∞	∞	1.9×10^{-5}	2870.1	2870.1	2.5×10^{-14}
0.25	12327.1	23463.9	3.7×10^{-10}	2701.0	2701.0	2.5×10^{-14}
0.286	12275.6	13466.2	1.3×10^{-12}	2581.4	2598.6	2.1×10^{-14}
0.333	13417.8	13417.8	1.4×10^{-12}	2601.8	2601.8	2.0×10^{-14}
0.4	∞	∞	1.3×10^{-1}	3008.4	3008.4	2.1×10^{-14}
0.5	∞	∞	3.2×10^{-1}	4564.3	4564.3	2.4×10^{-14}
0.6	∞	∞	6.7×10^{-1}	8604.5	9964.6	5.7×10^{-14}
0.7	∞	∞	1.5	∞	∞	5.3×10^{-2}

Figure 4: $T_{\max}$ versus μ for $\epsilon = 10^{-10}$, $T = 25000$ and $K = 10$.
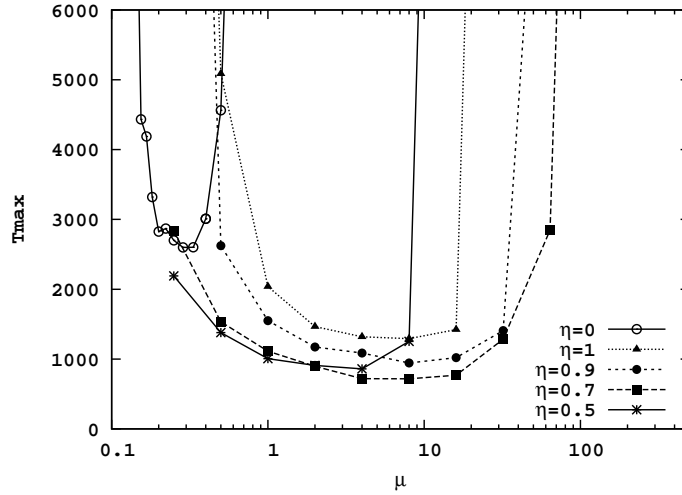
Next consider the family of smoothed interpolants $\tilde{I}_h$ for different values of η. Figure 4 plots $T_{\max}$ versus μ. When η is near 0.7 we find that values of μ between 1/4 and 64 all lead to approximations such that $\|u(t) - v(t)\|_V \leq 10^{-10}$ for large enough T. Thus, smoothing with η near 0.7 leads to a significantly wider range of values for μ such that the data assimilation algorithm can be

11

used to recover the reference solution. Note when $\eta = 2$ and $K = 10$ that no values of μ led to the convergence of the approximating solution to the reference solution over time.

Having found good values for η we continue our numerical study by fixing $\eta = 0.7$ and varying μ for different resolutions $h = L/K$, where $K = 8$, 9 and 10. As before $\epsilon = 10^{-10}$, $T = 25\,000$ and $T_0 = 2T/3$. The computational results given in Table 2 show that observational measurements with a resolution given by $K = 8$ can now lead to an approximate solution which converges to the reference solution over time. Moreover, the accuracy of the resulting approximations also improve compared to the non-smoothed case. Note that we have omitted reporting $T_{\min}$ in Table 2 since in all cases $T_{\min}$ was equal or nearly equal to $T_{\max}$.

Table 2: Data assimilation using $\tilde{I}_h$ where $\eta = 0.7$.

μ	$K = 8$		$K = 9$		$K = 10$	
	$T_{\max}$	$\varepsilon_{\mathrm{avg}}$	$T_{\max}$	$\varepsilon_{\mathrm{avg}}$	$T_{\max}$	$\varepsilon_{\mathrm{avg}}$
0.25	∞	5.1×10^{-1}	∞	9.9×10^{-2}	2834.2	2.4×10^{-14}
0.5	∞	6.5×10^{-2}	2570.1	2.4×10^{-14}	1534.2	1.7×10^{-14}
1	2817.8	1.1×10^{-13}	1686.5	1.8×10^{-14}	1112.7	1.6×10^{-14}
2	2527.1	2.6×10^{-14}	1232.6	1.7×10^{-14}	897.5	1.6×10^{-14}
4	2013.1	2.1×10^{-14}	1092.4	1.7×10^{-14}	718.9	1.6×10^{-14}
8	2191.6	2.1×10^{-14}	1124.8	1.7×10^{-14}	717.8	1.6×10^{-14}
16	4137.3	4.7×10^{-14}	1360.4	1.7×10^{-14}	769.7	1.6×10^{-14}
32	∞	3.0×10^{-1}	2752.9	2.1×10^{-14}	1284.2	1.7×10^{-14}
64	∞	1.4	∞	4.9×10^{-1}	2848.6	2.1×10^{-14}
128	∞	2.6	∞	1.9	∞	1.1

Figure 5 plots the data in Table 2. From this figure it is clear that the data assimilation algorithm given by (15) with I_h replaced by $\tilde{I}_h$ works well when $\eta = 0.7$ for a wide range of values of the relaxation parameter μ.

4   Numerical Methods

All fluid dynamics simulations presented in this paper were performed using a new parallel code written for the NVIDIA Compute Unified Device Architecture in the CUDA C programming language [16] which was developed on desktops at the University of Nevada Reno and run on the Big Red II Cray XE6/XK7 supercomputer at Indiana University. Computations were made in the stream function formulation using a fully-dealiased spectral Galerkin

12

Figure 5: $T_{\max}$ versus μ for $\epsilon = 10^{-10}$, $T = 25000$ and $\eta = 0.7$.
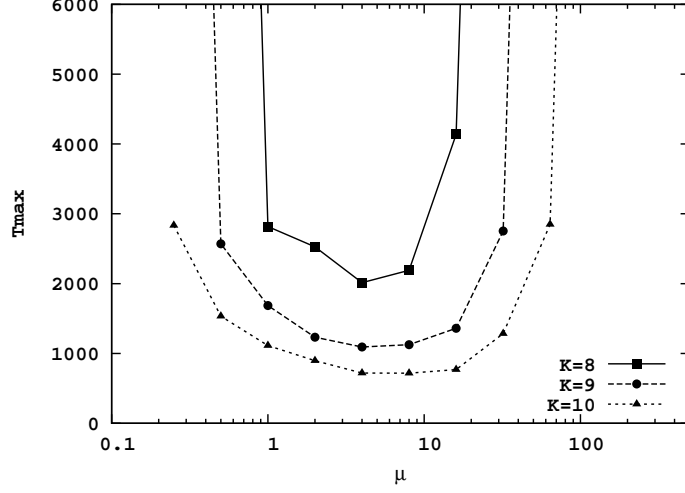
method. Time steps were performed using a split-Euler method in which the linear term was integrated exactly and the non-linear terms were integrated using forward differences.

Specifically we set $\Delta\Psi = \operatorname{curl} u$ and compute the reference solution using the stream function formulation

$$\frac{\partial \Delta\Psi}{\partial t} - \nu\Delta^2\Psi + \beta(\Psi) = \operatorname{curl} f, \tag{16}$$

where

$$\beta(\Psi) = J(\Psi, \Delta\Psi) = \Psi_x\Delta\Psi_y - \Psi_y\Delta\Psi_x$$
$$= ((\Psi_x)^2 - (\Psi_y)^2)_{xy} - (\Psi_x\Psi_y)_{xx} + (\Psi_x\Psi_y)_{yy}.$$

Similarly, set $\Delta\Phi = \operatorname{curl} v$ and compute the approximating solution using

$$\frac{\partial \Delta\Phi}{\partial t} - \nu\Delta^2\Phi + \beta(\Phi) = \operatorname{curl} f - \mu(R_h(\Phi) - R_h(\Psi)), \tag{17}$$

where $R_h(\Psi) = \operatorname{curl} P_\sigma I_h(\operatorname{curl}^{-1}\Delta\Psi)$. Note that $R_h: V^3 \to V^{-1}$.

Following the 2/3 dealiasing rule applied to 512×512 sized discrete Fourier transforms we set $\mathcal{K} = \{-341, \ldots, 341\}^2$ and approximate

$$\Psi \approx \sum_{k\in\mathcal{K}} \hat{\Psi}_k\, e^{ik\cdot x}, \quad \Phi \approx \sum_{k\in\mathcal{K}} \hat{\Phi}_k\, e^{ik\cdot x} \quad \text{and} \quad \operatorname{curl} f = \sum_{k\in\mathcal{K}} \hat{g}_k e^{ik\cdot x}.$$

Substituting these approximations into (16) and (17) and projecting onto the Fourier modes with wave numbers $k \in \mathcal{K}$ yields the Galerkin truncations

$$-\frac{d\hat{\Psi}_k}{dt}k^2 - \nu\hat{\Psi}_k k^4 + \hat{\beta}(\Psi)_k = \hat{g}_k$$

13

and

$$-\frac{d\hat{\Phi}_k}{dt}k^2 - \nu\hat{\Phi}_k k^4 + \hat{\beta}(\Phi)_k = \hat{g}_k - \mu\hat{R}_h(\Phi - \Psi)_k.$$

The corresponding numerical scheme for the reference solution is

$$\hat{\Psi}_k(t + \Delta t) \approx e^{-\nu k^2 \Delta t}\Big\{\hat{\Psi}_k(t) + \frac{\Delta t}{k^2}\hat{\beta}(\Psi(t))_k\Big\} - \frac{1}{\nu k^4}\hat{g}_k(1 - e^{-\nu k^2 \Delta t})$$

and for the approximating solution is

$$\hat{\Phi}_k(t + \Delta t) \approx e^{-\nu k^2 \Delta t}\Big\{\hat{\Phi}_k(t) + \frac{\Delta t}{k^2}\Big(\hat{\beta}(\Phi(t))_k + \mu\hat{R}_h(\Phi - \Psi)_k\Big)\Big\}$$
$$- \frac{1}{\nu k^4}\hat{g}_k(1 - e^{-\nu k^2 \Delta t}).$$

At the discrete level it is still the case that only nodal-point observational measurements of the reference solution are used to construct the approximating solution. Moreover, since both solutions are integrated using the same numerical methods, we may think of Ψ as an unknown reference solution that evolves according to a known discrete dynamical system, and the solution represented by Φ as an approximation generated by data assimilation according to the exact same discrete dynamics. Thus, even though our numerical schemes are only first order in time, we consider our numerical experiments to simulate data assimilation in the absence of both measurement and model errors.
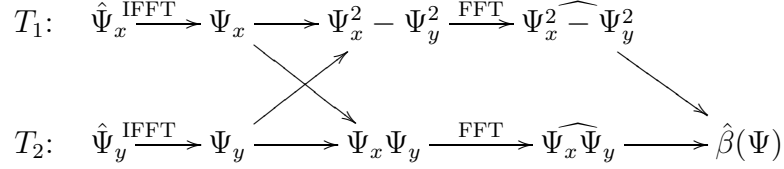
We take the time step to be $\Delta t = 1/2048$ which is enough to ensure that the CFL condition

$$\frac{N\Delta t}{2L}\sup_{x\in\Omega}\{|u_1(x)| + |u_2(x)|\} \leq 0.1608 \ll 1$$

is satisfied for the reference solution over the entire run. Note that as μ gets larger the data assimilation equations (15) become stiffer. Therefore, the time step Δt was also chosen small enough to ensure the stability of the coupled numerical scheme for computing the approximating solution.

Our numerical software has been optimized so that it runs entirely on the CUDA hardware with zero memory copies and four fast Fourier transforms per time step. Note that four transforms is the minimal number for the two-dimensional Navier–Stokes equations, see Basdevant [2] for further remarks and analogous optimizations when computing the three-dimensional Navier–Stokes equations. As device memory on the CUDA hardware is relatively scarce we also minimized our storage requirements. Storage requirements consist of four $n \times n$ double-precision scalar arrays: one for Ψ, another for

Figure 6: Data Flow for Computing the Non-linear Term

$$T_1: \quad \hat{\Psi}_x \xrightarrow{\text{IFFT}} \Psi_x \longrightarrow \Psi_x^2 - \Psi_y^2 \xrightarrow{\text{FFT}} \widehat{\Psi_x^2 - \Psi_y^2}$$

$$T_2: \quad \hat{\Psi}_y \xrightarrow{\text{IFFT}} \Psi_y \longrightarrow \Psi_x \Psi_y \xrightarrow{\text{FFT}} \widehat{\Psi_x \Psi_y} \longrightarrow \hat{\beta}(\Psi)$$

Φ and two temporary arrays T_1 and T_2. Figure 6 shows the data flow when computing the non-linear term. The first line represent the contents of T_1, the second represents T_2 and the arrows represent computational kernels.

When using 512×512 FFTs, our code achieves approximately 1062 time steps per second. In particular, the computational speed running on an NVIDIA Tesla K20 GPU was found to be roughly 37 times faster than equivalent CPU code running on single AMD Opteron 6212 core and 11.5 times faster when compared to running on 32 CPU cores. Correctness of operation was verified using the Navier–Stokes solver described in [17] and [18].

5 Conclusion

As is consistent with the analytical bound (8) and related discussion in [1], the numerical results given in Table 1 and Figure 5 show that the approximating solution does not converge to the reference solution when μ is either too small or too big. At the same time, provided the resolution h is fine enough and $\eta \approx 0.7$, there is a wide range of good values for μ when using the smoothed interpolant observable $\tilde{I}_h$. In particular, when $h = L/10 \approx 0.6283$, the data assimilation algorithm (7) performs similarly for values of μ between 0.5 and 32. Note, however, that smaller values of μ are computationally preferable because of stiffness considerations.

We remark that our numerical experiments have been conducted using exact error-free measurements and exact model dynamics and that in the presence of measurement and model errors we don't expect a similarly wide range of good values for μ. In fact, preliminary computations show when is noise added to the system that there exists a unique optimal value for μ reflecting the tradeoff between measurement and model errors. Theoretically, if the dynamics represented by $\mathcal{F}(u)$ in (1) are linear, then μ can be seen as the parameter of a linear Kalman filter, see for example Majda and Harlim [15], and there exists an analytically derived optimal value for μ which represents the tradeoff between measurement and model errors. In the fully non-linear case studied here, the fact that there is a wide range of good constant values for μ in the absence of measurement and model errors suggests, provided the

15

resolution h is fine enough, that μ can be further optimized as if the model was linear.

We now compare the coarsest resolution $h = L/K$ that works for the data assimilation experiments presented here when $\eta = 0.7$ to the number of numerically determining modes found in [18]. Under the same physical parameters and forcing, the minimum number of Fourier modes needed by (2) was

$$n_c = \operatorname{card}(\mathcal{D}_5) = 80$$

where

$$\mathcal{D}_R = \{\, e^{ik \cdot x} : 0 < k_1^2 + k_2^2 \le R^2 \,\}.$$

In this paper we show the minimum of nodal measurements needed are

$$N = K^2 = 64$$

which by the Nyquist–Shannon sampling theorem may be represented by the Fourier modes

$$\mathcal{N}_K = \{\, e^{ik \cdot x} : 0 < \max(|k_1|, |k_2|) \le K/2 \,\}.$$

To compare these two results we note that $\mathcal{D}_R$ represents a circle in Fourier space while $\mathcal{N}_K$ represents a square. Let $R_{\min} = 5$ and $K_{\min} = 8$. If the resolution requirements of algorithm (2) are comparable to (7), we would expect that $\mathcal{N}_{K_{\min}} \subseteq \mathcal{D}_R$ would imply $R \ge R_{\min}$ and that $\mathcal{D}_{R_{\min}} \subseteq \mathcal{N}_K$ would imply $K \ge K_{\min}$. This is supported by our results. If $\mathcal{N}_8 \subseteq \mathcal{D}_R$ then

$$R \ge \frac{8\sqrt{2}}{2} \approx 5.65 \ge 5 = R_{\min}.$$

Similarly, if $\mathcal{D}_5 \subseteq \mathcal{N}_K$ then

$$K \ge 2 \cdot 5 = 10 \ge 8 = K_{\min}.$$

Thus, even though our nodal observations possess the problems of aliasing and high-frequency spill over, these problems can be mediated with appropriate smoothing. The resulting resolution K needed for the approximating solution to converge to the exact solution is then about the same as suggested by the number of numerically determining modes.

Acknowledgements

References

[1] A. Azouani, E. Olson, E.S. Titi, Continuous data assimilation using general interpolant observables, Journal of Nonlinear Science, Vol. 24, 2014, 277–304.

[2] C. Basdevant, Technical Improvements for Direct Numerical Simulation of Homogeneous Three-Dimensional Turbulence, Journal of Computational Physics, Vol. 50, 1983, pp. 209–214.

[3] H. Bessaih, E. Olson, E.S. Titi, Continuous Data Assimilation with Stochastically Noisy Data, *Nonlinearity*, Vol. 28, 2015, pp. 729–753.

[4] D. Blömker, K. Law, A.M. Stuart, K.C. Zygalakis, Accuracy and stability of the continuous-time 3DVAR filter for the Navier-Stokes equation.

[5] J. Charney and M. Halem and R. Jastrow, Use of incomplete historical data to infer the present state of the atmosphere, *J. Atmos. Sci.*, Vol. 26, 1160–1163.

[6] P. Constantin, C. Foias, *Navier–Stokes Equations*, University of Chicago Press, 1988.

[7] A. Farhat, M.S. Jolly, E.S. Titi, Continuous data assimilation for 2D Bénard convection through velocity measurements alone, *Physica D*, to appear.

[8] A. Farhat, E. Lunasin, E.S. Titi, Abridged dynamic continuous data assimilation for the $2D$ Navier-Stokes equations. *arXiv*:1504.05978 [Math.AP]

[9] C. Foias, R. Temam, Determination of the solutions of the Navier-Stokes equations by a set of nodal values, *Math. Comp.*, Vol. 43, No. 167, 1984, pp. 117–133.

17

[10] M. Gesho, *A Numerical Study of Continuous Data Assimilation Using Nodal Points in Space for the Two-dimensional Navier–Stokes Equations*, Masters Thesis, University of Nevada, Department of Mathematics and Statistics, 2013.

[11] M. Jolly, V. Martinez, E.S. Titi, A data assimilation algorithm for the subcritical surface quasi-geostrophic equation. Preprint.

[12] D.A. Jones, E.S. Titi, Upper bounds on the number of determining modes, nodes and volume elements for the Navier–Stokes equations, *Indiana Univ. Math. J.*, Vol. 42, No. 3, 1993, pp. 875–887.

[13] E. Kalnay, *Atmospheric modeling, data assimilation and predictability*, Cambridge University Press, 2003.

[14] K. Law, A. Shukla, A. Stuart, Analysis of the 3DVAR filter for the partially observed Lorenz'63 model. *Discrete Contin. Dyn. Syst.* vol. 34, no.3, 2014, pp. 1061–1078.

[15] A. Majda, J. Harlim, *Filtering Complex Turbulent Systems*, Cambridge University Press, 2012.

[16] *CUDA C Programming Guide*, www.nvidia.com, 2012, pp. 1–175.

[17] E. Olson, E.S. Titi, Determining modes for continuous data assimilation in 2D turbulence, *Journal of Statistical Physics*, Vol. 113, No. 5–6, 2003, pp. 799–840.

[18] E. Olson, E.S. Titi, Determining modes and Grashof number in 2D turbulence, *Theoretical and Computational Fluid Dynamics*, Vol. 22, No. 5, 2008, pp. 327–339.

[19] J. Robinson, *Infinite-Dimensional Dynamical Systems*, Cambridge Texts in Applied Mathematics, 2001.

[20] R. Temam, *Navier–Stokes Equations and Nonlinear Functional Analysis*, CBMS Regional Conference Series, No. 41, SIAM, Philadelphia, 1983.

[21] Z. Xiao, M. Wan, S. Chen, G. Eyink, Physical mechanism of the inverse energy cascade in two-dimensional turbulence: a numerical investigation, *J. Fluid Mech.*, Vol. 619, 2009, pp. 1–44.